Excitation in low-current discharges and breakdown in He at low pressures and very high electric field to gas density ratios E/N

B. M. Jelenković*
JILA, University of Colorado and National Institute of Standards and Technology, Boulder, Colorado 80309-0440, USA and Institute of Physics, P.O. Box 75, Belgrade, Serbia and Montenegro

A. V. Phelps
JILA, University of Colorado and National Institute of Standards and Technology, Boulder, Colorado 80309-0440, USA
(Received 1 August 2004; published 26 January 2005)

We investigate optical emission from low-current discharges in He at very high electric field to gas density ratios E/N between parallel plate electrodes. We also determine the electrical breakdown and the voltage-current behavior at low currents. The E/N are 300 Td to 9 kTd (1 Td$=10^{-21}$ V m^2) at pressures times electrode separations p_0d from 3 to 0.9 Torr cm. Absolute optical emission probabilities versus distance are determined for the 501.6 nm line ($3\,^1P \rightarrow 2\,^1S$) and for the 587.6 nm line ($3\,^3D \rightarrow 2\,^3P$) by reference to Boltzmann calculations at our lowest E/N and to published pressure dependent electron beam experiments. At E/N below 1 kTd, the emission follows the exponential growth of the electron density, while at above 7 kTd heavy particle excitation is evident near the cathode. Collisional transfer of excitation from the singlet to the triplet system dominates the 587.6 nm excitation. Comparisons of models with experiments show the importance of excitation and of electron production at the cathode by fast He atoms produced by charge transfer collisions of He^+ with He. The breakdown voltage versus p_0d is multivalued for $p_0d \sim 1.5$ Torr cm. At currents below 100 μA and our lower E/N, the discharge voltage decreases linearly with current as expected for an increasing electron yield with ion energy and E/N at the cathode.

DOI: 10.1103/PhysRevE.71.016410 PACS number(s): 52.20.Hv, 34.20.−b, 34.50.−s

I. INTRODUCTION

This research is an extension to He of our previously reported measurements and analyses of the radiation emitted by low current discharges in N_2 [1,2], Ar [3,4], and H_2 [5] at very high electric field to gas density ratios E/N and low gas densities. The previous papers on N_2 will be referred to as I and II, respectively, and those on Ar as III and IV. One reason for selecting the rare gases is that models [3] of positive ion and fast neutral behavior are much simpler for Ar and He than for N_2 and H_2. We will show that by constructing a reasonably complete model of He^+ ion and fast He atom motion, including excitation by the fast He atoms, we can obtain approximate fits to the spatial dependence of emission and electrical breakdown voltage data at the higher E/N. Emission measurements similar to these, but at lower E/N, have been carried out by Petrović and co-workers [6].

The spatially uniform electric field experiments reported in this paper are concerned with electron and ion motion for the product of pressure (normalized to 273 K) times electrode separation (p_0d) ranging from values where there are sufficient collisions to allow one to describe the electron motion in terms of the steady state motion at the local electric field to gas density ratio E/N to low p_0d where there are few collisions and nonequilibrium effects are important. We will refer to models appropriate to these two limits as the local field and nonequilibrium models, respectively. Nonequilibrium phenomena result in a spatial dependence of the electron energy distribution. Experiment and theory [7] have shown that even at low E/N, nonequilibrium effects cause oscillatory structure in the excitation and ionization rates after the electrons leave the cathode but before they can be described by the local field model. Details of the approach to this steady state have been calculated for electrons in He with a dc uniform electric field using Monte Carlo techniques [8–13], spherical harmonic and density-gradient expansion techniques [12,14,15], and other approaches [10,14,16]. The experimentally observable results of these calculations include the distance (d_0) or voltage change (V_0) required for the electron excitation and/or ionization coefficients to become independent of position. Monte Carlo calculations [9] for He yield $p_0d_0=1.3$ Torr cm at $E/N=56$ Td, but show that for E/N greater than about 850 Td a steady state energy distribution is not reached, i.e., the electrons appear to undergo "runaway." Here 1 Td$=10^{-21}$ V m^2 and 1 Torr$=133$ Pa. Experiments [11,17,18] give larger than calculated values of p_0d_0 at low E/N, but agree that a constant ionization rate is not reached for $p_0d=1$ Torr cm for $E/N=850$ Td. The corresponding V_0 values required for use of the local field model in He are much larger than values found for the heavier rare gases [7], because of higher inelastic thresholds and lower excitation and ionization cross sections for He.

At the lower E/N (<1 kTd) considered in the present paper, the electrons reach a steady state distribution in the electric field long before striking the anode and the local field models of electron behavior apply except very close to the electrodes. Local field models can then be used for analyses of ionization growth and electrical breakdown in He and

*Present address: Jet Propulsion Laboratory, Pasadena, CA 91109.

will be used for calibration of our excitation rates. Experimental and theoretical studies yield spatially independent ionization coefficients [7,8,17,19–25] and electron yields per positive ion striking the cathode [7,13,26,27]. Spatially independent excitation coefficients for electrons in He have been calculated [19–21].

At our higher E/N (>4 kTd), models of electric breakdown must treat the electrons using nonequilibrium models. Parker and colleagues [28] used Monte Carlo techniques to simulate the production of ionization by electrons and ions, the reflection of electrons from the anode, and the release of electrons from the cathode by ions. They were able to obtain the multivalued behavior of the breakdown voltage versus p_0d observed in He [7]. The production of electrons at the cathode by He metastables is not important here because of their relatively small production by electrons at very high E/N, e.g., ≈5% of ionization at $E/N=300$ Td [21]. Resonance photon excitation is comparable with ionization [21], but its contribution to electron ejection at the cathode is reduced by imprisonment effects [19] and low electron yields per photon [29]. The contribution of the release of electrons from the cathode by fast atoms and of the ionization of He by fast ions has been demonstrated for breakdown by Hartmann *et al.* [13].

Much less work has been concerned with nonequilibrium effects for positive ions in uniform electric fields. Theory has predicted the distances required for velocity distributions to relax to their equilibrium form for ions in their parent gas [30] and for foreign gas ions [31–33]. For the case of He^+ in He, the predicted ion energy relaxation distance corresponds to $p_0d\approx 0.01$ Torr cm and is slowly varying with ion energy and E/N [34]. Measurements of ion energy distributions at the cathodes of low current, uniform field discharges in He by Rao, Van Brunt, and Olthoff [35] show good agreement with calculated energy distributions assuming local field equilibrium for $E/N<20$ kTd and for $p_0d>1$ Torr cm, thereby including our experimental conditions. Townsend and Yarnold [36] have reported spatial ionization coefficients for He^+ collisions with He at E/N from 100 to 200 Td and p_0d from 8 to 2 Torr cm, but we will see that their values seem much too large.

In spite of the nonuniform electric fields, some studies of the cathode fall of discharges in rare gases [7,30,37–42] are relevant to the present work, because of their conclusion that neutral heavy-particle effects are important. Davis and Vanderslice [38] measured the ion energy distributions from the He cathode fall, but neutral energy distributions measurements [40] appear to have not been measured for discharges in He. A number of authors [30,38–41] have calculated these distributions. The importance of a proper accounting for the fast neutral atoms has been emphasized by several authors [37,39–41], primarily because they are sources of secondary electrons and of cathode sputtering. In particular, Neu [37] showed that his models of the cathode fall in He required that fast He atoms produce many of the electrons at the cathode. Very recently, Hartmann *et al.* [43] have demonstrated that a very high fraction (75%) of the electron emission from the cathode can be caused by fast neutral atoms.

Because of the extensive discussion in papers I and II of the experimental apparatus and techniques used in the present work, we will give only brief summaries of these topics in Sec. II. In Sec. III we describe models for the electron, ion, and fast atom motion and for the resultant production of excited atoms and ionization. We also summarize available cross section data. The predictions of the electron-ion-atom model of He excitation will be compared with experiment in Sec. IV. In Sec. V we compare the predictions of various models of ionization with the measured breakdown and discharge maintenance voltages. An abstract summarizing this work has been presented previously [44].

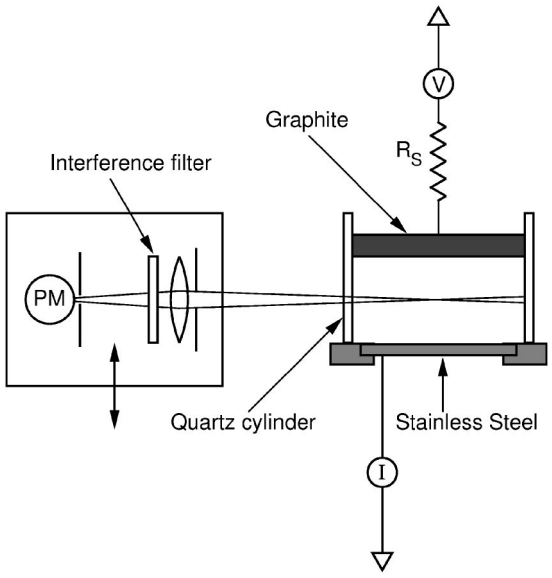

FIG. 1. Schematic of experiment. Unless otherwise stated, the stainless steel electrode was the cathode and the graphite electrode was the anode.

II. EXPERIMENT AND RESULTS

The experimental apparatus and techniques were discussed in detail in I and will only be summarized here. A schematic of the drift tube and optical scanning device are shown in Fig. 1. The discharge is operated between parallel plane electrodes separated by ceramic spacers of length 9.3 mm. Normally the sintered graphite electrode [45] is the anode and the stainless steel electrode is the cathode. The electrodes are 80 mm in diameter and are surrounded by a close-fitting quartz tube to prevent long path breakdown. For the emission measurements, the discharges are operated at currents of ~3 μA (2.5×10^{-5} A/m^2) at low E/N and ~8 μA at high E/N. The low currents prevent significant space-charge distortion of the spatially uniform electric field and eliminate nonlinear effects such as gas heating and collisions among excited and/or charged species. The discharge current in our experiments is limited by an external resistor, typically 1 MΩ, between the cathode and a stabilized voltage supply. The current is monitored and measured using an operational amplifier between the anode and ground. The discharge operating voltage is essentially independent of current for the current densities used of less than 10^{-4} A/m^2, so that the discharges can be characterized by the values of operating voltage versus p_0d.

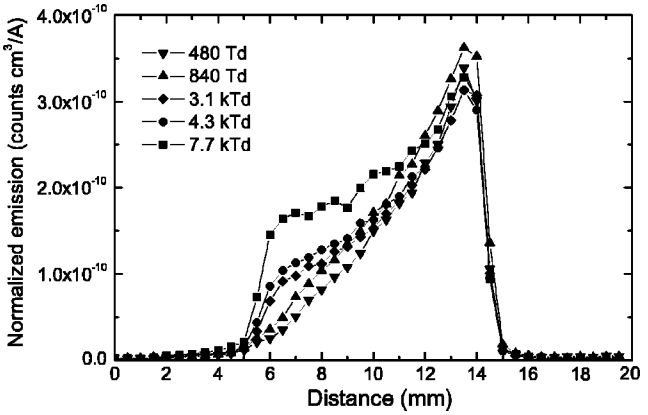

FIG. 2. Measured 501.6 nm emission from He $3\,^1P$ state, normalized to current and gas density, for E/N from 480 Td to 7.7 kTd. The symbols, voltages in V, and pressures in Torr for these data are ▼, 250, 1.7, ▲, 386, 1.5, ◆, 1397, 1.45, ●, 1785, 1.35, and ■, 2490, 1.05.

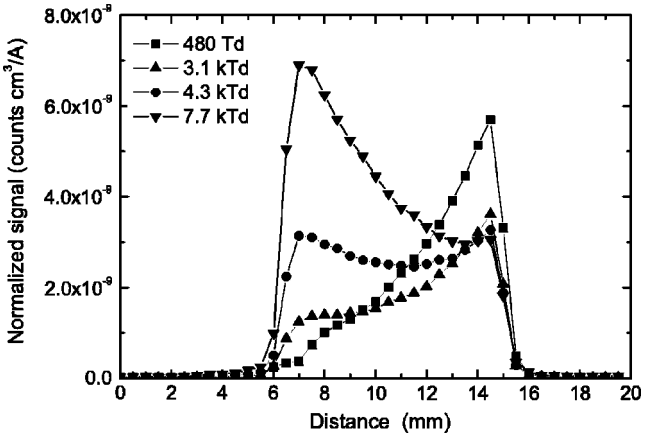

FIG. 3. Measured 587.6 nm emission from He $3\,^3D$ state, normalized to current and gas density, for E/N from 300 Td to 8.8 kTd. The symbols, voltages in V, and pressures in Torr for these data are ■, 340, 1.49, ▲, 1240, 1415, ●, 1955, 1.21, and ▼, 2590, 0.96.

The helium is stated by the manufacturer to be 99.999% pure, so that for our experiments the principal contamination is from the rate of rise of the system background pressure of less than 10^{-2} Pa/min. This means that for an hour long run and for an excited state quenching rate coefficient for impurities of 10^{-15} m^3/s, less than 5% of the excitation of importance to the models of Sec. III is lost to quenching by impurities. The rate coefficient for charge transfer from He^+ to N_2, CO, and H_2 are 1.5×10^{-9}, 1.9×10^{-9}, and $<10^{-13}$ cm^3/s at 300 K [46]. At low E/N, the low drift velocities of He^+ in He may well lead to significant loss of helium ions to N_2 and CO by charge transfer. However, ion conversion processes have no effect on the magnitude and spatial dependence of the dominant electron excited emission. Because of the short ion transit times at high E/N, ion conversion is improbable and will be neglected.

The electrodes were chemically cleaned in an ultrasonic bath. After evacuation, the electrodes were mildly sputtered using a H_2 discharge for ~10 min at a current of less than ~1 mA, chosen to avoid constrictions.

Observed spatial distributions of intensities for the 501.6 nm and 587.6 nm lines, normalized to the gas density and discharge current, are plotted versus position in Figs. 2 and 3 for E/N values from 300 Td to 9 kTd. The results were found to be independent of current over factors of two in current. The spatial scans were made using interference filters. The photomultiplier used [3] had a GaAs(Cs) photocathode so that we expect the quantum efficiency to be roughly 30% lower at 587.6 nm than at 501.6 nm. The normalized signals are in arbitrary units because of changes in discriminator settings and photomultiplier voltages between runs. These changes between runs do not enter into our calibration procedure.

The "high spatial resolution" slits described in I are used and yield approximately 1 mm resolution. Data are obtained at the p_0d values and voltages V_d shown in the legends for Figs. 2 and 3. The measured operating voltages differ little from values obtained by extrapolation to zero current. The variation of discharge voltage with current, presented in Sec. V, are obtained using both steady state and pulsed measurements [47]. The smaller apparent electrode separations in Figs. 2 and 3 than the nominal 9.3 mm are, in part, caused by the nonequilibrium effects near the electrodes discussed in Sec. III B. Reversals of the electrode voltages, carried out at low E/N, give nearly mirror images of the normalized emission signals.

As found by several authors [48] for H_2, Ne, Kr, and Xe, by us in I for N_2, and in II for Ar, the optical emission at $E/N<1000$ Td increases exponentially with distance from the cathode for most of the electrode gap. The departure from the exponential growth near the cathode at the lowest E/N is indicative of the initial nonequilibrium behavior of the electrons discussed in Sec. III. The spatial ionization (Townsend) coefficients derived from the exponential growth of emission in Figs. 2 and 3 are shown by the solid circles and diamonds in Fig. 4. The uncertainties in the determination of ionization coefficients increase with E/N because of difficulties in separating the contributions of electron-induced emission and heavy particle emission in the spatial distributions of Figs. 2 and 3, especially for the 587.6 nm data [49].

We next discuss the assumptions and procedure used in the normalization of emission data of Figs. 2 and 3. We assume that at the anode there is negligible electron-induced emission of ions [50] at low E/N, so that the measured total current is equal to the electron current at the anode. Thus, the emission extrapolated to the anode is produced by electrons having a current density equal to the measured total current density. We also assume negligible ion and excited state production by backscattered electrons at low E/N. For each transition, we normalize the measured emission count rate $S\{j,(E/N),N,z\}$ to the theoretical electron excitation coefficients α_x/N discussed in Sec. III B. The apparent electron excitation coefficient as a function of position [1] $\beta_x/N(z,E/N)$ at an arbitrary E/N is related to the position-independent $\alpha_x/N(E/N)_r$ at the reference $(E/N)_r$ by

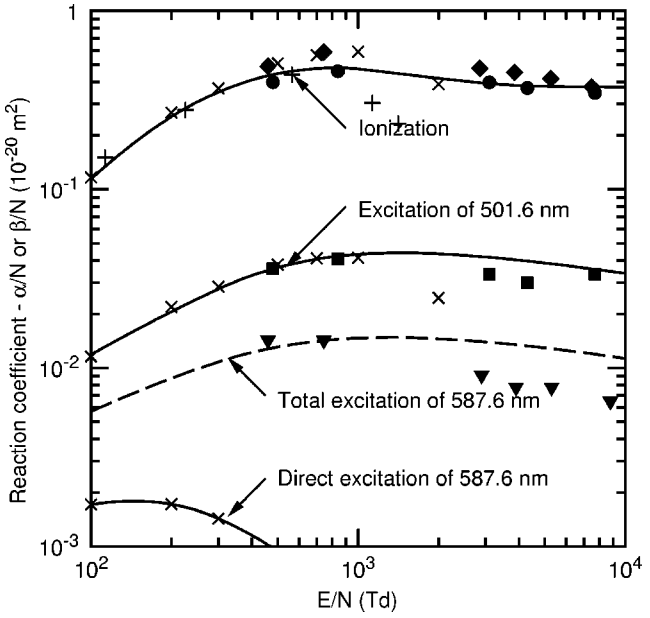

FIG. 4. Ionization coefficient α_i/N and excitation coefficient α_x/N for electrons in He. The values used in our local field model are shown by the solid and dashed curves. The ionization coefficients obtained from the 501.6 and 587.6 nm emission profiles are shown by ● and ♦. The excitation coefficients obtained by extrapolation of the normalized emission to the anode and corrected for quenching are shown by ■ and ▼. Our Boltzmann and Hayashi's Monte Carlo results are shown by × and +, respectively.

$$\frac{\beta_x}{N}(z,E/N) = \left[\frac{S\{j,(E/N),N,z\}}{S\{j_r,(E/N)_r,N_r,d\}}\right]\left[\frac{j_r N_r}{jN}\right] \times \left[\frac{(1+N/N_q)}{(1+N_r/N_q)}\right]\frac{\alpha_x}{N}(E/N)_r, \quad (1)$$

where j is the radially averaged, total current density, z is the distance from the cathode and d the electrode separation, N_q is the gas density such that 50% of the emission is quenched before emission, and r is used to designate parameters appropriate to the reference conditions. $S\{j,(E/N),N,z\}$ is the signal measured at the position z, and $S\{j_r,(E/N)_r,N,d\}$ is the measured signal after extrapolation to the anode under the reference conditions at our lowest $(E/N)_r$. At low E/N the spatial dependence of the apparent excitation coefficients reflects the growth of the electron flux by ionization, while the magnitude includes direct excitation by electrons and production by cascading and excitation transfer. At higher E/N, the spatial dependence of the apparent excitation coefficients includes contributions from excitation by electrons of the electron-ion avalanche, electrons reflected from the anode, fast atoms, fast ions, and by excitation transfer. These processes will be discussed below, as will the appropriate collisional quenching. As will be discussed in Sec. III E, the presence of the the quenching correction factors in Eq. (1) means that for our conditions α_x/N is a function of E/N but not the He density N. The calibration procedure for the detection system represented by Eq. (1) will be applied to experimental data from Figs. 2 and 3 in Sec. IV.

III. THEORY OF EXPERIMENT

In this section we present simplified models of electron, ion, and fast atom production, transport, and collisions. We also present the resultant excitation of 501.6 nm and 587.6 nm emission. We will apply this model in Sec. IV. For the electrons at low E/N, we use a local field model with reaction coefficients from time-independent, spatially growing, two-term solutions to the Boltzmann equation. For high E/N, we test the applicability of three different models for electrons. Because of the short relaxation lengths for He^+ in He at our pressures, the He^+ ions are always modeled using a local field model. We neglect He_2^+ and He^{2+} formation [35]. Because of our large electrode diameter to electrode separation ($\approx 9:1$), we consider a one-dimensional, uniform electric-field model with the z axis parallel to the drift tube axis and perpendicular to the electrodes.

A. Local field model for electrons

The measurements of excitation utilized for calibration are for E/N below about 800 Td, so that the electron behavior can be analyzed using the equilibrium or local field model for electrons. The electron flux density $\Gamma_e(z)$ and the He^+ ion flux density $\Gamma_+(z)$ are given by the solutions to the differential equations

$$\frac{d\Gamma_e(z)}{dz} = \alpha_{ie}(z)\Gamma_e(z) + \overline{Q_+^i}(E/N)N\Gamma_+(z) + \overline{Q_f^i}(E/N)N\Gamma_f(z) \quad (2)$$

and

$$\frac{d\Gamma_+(z)}{dz} = -\frac{d\Gamma_e(z)}{dz}, \quad (3)$$

where $\alpha_{ie}(z)/N$ is the spatial (Townsend) coefficient for ionization by electrons and z is measured from the cathode toward the anode.

An approximate allowance is made for nonequilibrium effects near the cathode [7,29], i.e., a delay in the onset of ionizing collisions and a reduction in the electron yield per incident ion or fast atom attributed to scattering of the electrons back to the cathode. Here we assume that $\alpha_e^i(z)/N$ is zero for $z < d_0$, and for $z > d_0$ is given by

$$\alpha_e^i(E/N) = (2e/m)N/W_e(E/N)\int_0^\infty \epsilon Q_e^i(\epsilon) f(\epsilon,E/N)d\epsilon. \quad (4)$$

Here e and m are the electron charge and mass, $Q_e^i(\epsilon)$ is the cross section for ionization of He by electrons, $f(\epsilon,E/N)$ is the equilibrium electron energy distribution, $\Gamma_+(z)$ and $\Gamma_f(z)$ are the He^+ and fast atom fluxes, and $W_e(E/N)$ is the electron drift velocity. $\overline{Q_+^i}(E/N)$ and $\overline{Q_f^i}(E/N)$ are the average cross sections for ionization of He by He^+ ions and by fast He atoms, respectively. The calculation of the coefficients and average cross sections is discussed in Secs. III F through III H.

Because of our use of a graphite anode for the quantitative emission measurements, we neglect electron reflection at the

anode and assume that $\Gamma_e(d)$ is equal to the total current density Γ_t. At the cathode at $z=0$

$$\Gamma_e(0) = \gamma_i(E/N)\Gamma_+(0) + \gamma_f(E/N)\Gamma_f(0), \tag{5}$$

where the electron yield per ion γ_i and the electron yield per fast atom γ_f are expressed as function of E/N because of the local field equilibrium for the energy distribution for He^+ ions and the fast He atoms produced by charge transfer. These γ coefficients include the effects of electron backscattering to the cathode by the gas atoms. When solving these equations numerically, we take the origin at the anode, where the electron-induced ion and fast-atom fluxes can be assumed to be negligible [50].

At low E/N, we neglect ionization of He by He^+ and fast atoms and approximate the initial nonequilibrium effects [7,29] by assuming that there is no ionization by electrons for $z<d_0$. Using Eqs. (2) and (3), the solution for the electron flux for $z \geqslant d_0$ is

$$\Gamma_e(z) = \Gamma_e(0)\exp[\alpha_{ie}(z-d_0)]. \tag{6}$$

The corresponding solution for the He^+ ion flux for $z \geqslant d_0$ is

$$\Gamma_+(z) = \Gamma_e(0)\exp[\alpha_{ie}(d-d_0)](1-\exp[-\alpha_{ie}z]). \tag{7}$$

For $z<d_0$, the ion flux is constant at

$$\Gamma_+(z) = \Gamma_e(0)\{\exp[\alpha_{ie}(d-d_0)]-1\}. \tag{8}$$

We assume $V_0 \equiv d_0E = 25+10/(E/N)$ from [7]. Here V_0 is in V and E/N is in Td.

At very high E/N, there is the possibility of current growth as the result of ionization by electrons and fast ions only, as originally proposed by Townsend [51,52]. In this case, the solution to Eqs. (2)–(5) is

$$\Gamma_e(z) = \Gamma_e(0)\frac{(\alpha_{ie}-\alpha_{i+})\exp[(\alpha_{ie}-\alpha_{i+})z]}{\{\alpha_{ie}-\alpha_{i+}\exp[(\alpha_{ie}-\alpha_{i+})z]\}}, \tag{9}$$

where Townsend's α_{i+} is the same as $\overline{Q_+^i}(E/N)N$ in Eq. (2). Here we have followed the custom of assuming that $d_0 \ll d$, so that the effects of the nonequilibrium region near the cathode can be neglected.

B. Nonequilibrium models for electrons

The local field model is questionable for electrons at our higher E/N and we have tried two different approximations as nonequilibrium models. Our first approach is the "single-beam" moment method described in III and successfully applied to electrons Ar in IV. This single-beam model treats the energy loss caused by excitation and ionization processes as frictional forces acting on a monoenergetic beam. In addition, the new electron produced by ionization is added to the beam flux and the total beam energy is reduced by the energy of the new electron. Because of the small excitation and ionization cross sections for electrons in He and the large energy gain per mean-free-path for our high E/N, this model resulted electrons in nearly free-fall motion and produced excitation only very near the cathode. This is contrary to the data of Figs. 2 and 3.

Our second approach was also a moment method but assumes a one-dimensional Maxwellian distribution. The derivation adapts the ideas of Lawler [30] for ions moving in their parent gas in which symmetric charge transfer collisions produce an ion with zero kinetic energy. In the present case, ionizing collisions at high incident energies (>100 eV) produce one electron at an energy relatively near to zero and one electron that has lost an energy not much larger that the ionization potential [53]. In our model, the low energy electron is treated as a delta function source at zero energy and the loss of energy by the high energy electron is treated as a frictional force. Other inelastic losses are treated as friction. Because of the high "temperatures" characterizing the electron distribution at high E/N, the friction terms caused by energy loss in elastic recoil scattering and by energy loss in excitation and ionization turn out not to be very important in this model. The acceleration of electrons produced by ionization from zero energy to the mean energy corresponding to the temperature of the distribution dominate the energy loss. This feature is present in early descriptions of electron motion in hydrogen [54]. Because of the one-dimensional, beamlike behavior of the electron velocity distribution, this approach gives significantly fewer ionization and excitation collisions than, for example, the three-dimensional Maxwellian usually used in moment methods. We have not attempted the Monte Carlo modelings necessary to evaluate the relative merits of the various models theoretically but will compare model predictions with experiment in Sec. IV.

In the one-dimensional Maxwellian case, Eq. (2) is replaced with equations from the zeroth moment and second moment of the electron Boltzmann equation with the unknown temperature $kT_e[Z]$ and electron-flux density $j_e[z]$ as functions of position. These equations correspond to the number and energy balances. Starting with the appropriate form of the Boltzmann equation [30] and taking velocity moments, we obtain

$$\frac{d\Gamma_e(z)}{dz} = Q_e^i(2,kT_e(z))N\Gamma_e(z) + \overline{Q_+^i}(E/N)N\Gamma_+(z) + \overline{Q_f^i}(E/N)N\Gamma_f(z) \tag{10}$$

and

$$\Gamma_e(z)E = \frac{d}{dz}[kT_e(z)\Gamma_e(z)] + \frac{1}{4}\epsilon_i N\Gamma_e(z) \times [2Q_e^i(3,kT_e(z)) - Q_e^i(1,kT_e(z))], \tag{11}$$

where

$$Q_e^i(h,kT_e(z)) = [\Gamma(h/2+1/2)]^{-1}[kT_e(z)]^{-(h+3)/2} \times \int_0^\infty \epsilon^{(h+1)/2}Q_e^i(\epsilon)\exp[-\epsilon/kT_e(z)]d\epsilon. \tag{12}$$

Here ϵ is the electron energy, $Q_e^i(\epsilon)$ is the electron-He ionization cross section with an energy loss equal the ionization energy ϵ_i, and $\Gamma(m)$ is the gamma function. The normalization of $Q_e^i(h,kT_e(z))$ in Eq. (12) is chosen such that for $Q_e^i(\epsilon)=Q_e^i$ independent of energy, $Q_e^i(h,kT_e(z))=Q_e^i$ for all h.

Equation (10) is the equivalent of Eq. (2). Equation (11) is an energy balance with the power input equal to the sum of the energies required to heat new electrons and to supply inelastic losses to ionization. We have neglected energy losses to excitation, as justified by our tests. Here kT_e is in electron volt units. The cross sections used are discussed in Sec. III F.

C. Model for He^+ ions

Our model for the He^+ ions is the steady state limit of the symmetric charge-transfer model [3,30]. The He^+ flux is determined by Eq. (3). The "temperature" of the one-dimensional Maxwellian energy distribution is $kT_+ = q_e(E/N)/\overline{Q}_{CT}$ and the He^+ drift velocity is $W_+ = [2q_e(E/N)/(M_+\overline{Q}_{CT})]^{1/2}$. Here $\overline{Q}_{CT}(E/N)$ is the average of the symmetric charge-transfer cross section for $He^+ + He$ and varies slowly with ion energy, q_e is the electron charge, and M_+ is the He^+ mass. An empirical fit to experiment [55] gives

$$kT_+ = 4[(E/N)/1000]^{1.2}, \tag{13}$$

where kT_+ is in eV and E/N is in Td.

D. Model for fast He atoms

Our approximate model for the effects of fast atoms assumes (a) that because the fast atoms are produced by symmetric charge-transfer collisions they have the same velocity distribution as the steady state distribution of the He^+ ions [3,30] and (b) that any elastic viscosity or inelastic collision results in destruction of the fast atom by reducing its energy below the range of observable excitation or ionization effects. This model is similar to that used with reasonable success for excitation by fast Ar atoms in Ar [3]. The equation for the fast atom flux is

$$\frac{d\Gamma_f(z)}{dz} = \overline{Q}_{CT}(E/N)N\Gamma_+(z) - \sum k\overline{Q}_f^k(E/N)N\Gamma_f(z), \tag{14}$$

where $\overline{Q}_f^k(E/N)$ is the average cross section for the kth elastic or inelastic process. These averages over the one-dimensional ion energy distribution [3] are given by Eq. (12) for $h=-1$. The values of kT_+ are converted to E/N using Eq. (13), where ϵ is the fast atom energy in laboratory coordinates. The cross sections used are discussed in Sec. III H.

E. Model for excited He atoms

Our model for the He($3\,^1P$) excited atom density is an extension of that of Jobe and St. John [56,57] to higher pressures as shown in Fig. 5. The points show the experimental [57] line-excitation cross sections at 100 eV. The results of models [57,58] taking into account the self-absorption (imprisonment) of the 53.7 nm resonance line emitted by the He($3\,^1P$) state in transitions to ^1S ground state is shown by the heavy smooth curve. In general, the apparent excitation cross section increases from its direct excitation value at very low gas densities toward a limiting value for optically thick resonance line and no quenching. The accuracy of this extrapolation is estimated [57] to be better than ±25%. The

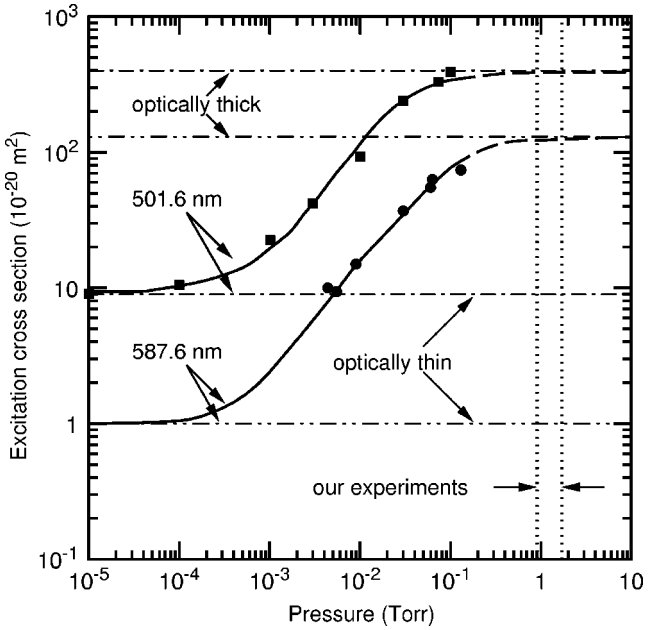

FIG. 5. Line excitation cross sections for the 501.6 and 587.6 nm lines of He by 100 eV electrons as a function of He pressure. The experimental points shown are from Jobe and St. John [57]. The theoretical curves and horizontal limiting values are discussed in the text. The vertical dotted lines indicate the pressure range of our emission experiments.

portions above 0.1 Torr are shown dashed to emphasize the point that the models for He do not include the effects of collisional quenching. Because there is almost complete imprisonment at our pressures [59,93], we will not review the imprisonment model here. The effects of collisional quenching, using published reaction data [56,60], will be accounted for using the model of the next paragraph.

The model used to calculate the spatially dependent 501.6 nm emission takes into account the production of $3\,^1P$ atoms by electrons, fast atoms, and ions, the loss by 501.6 nm radiation to the $2\,^1S$ metastable state, production by radiative decay from higher levels, collisional excitation transfer to nearby or lower energy levels, and molecular ion formation. At our pressures, the loss of excitation by resonance radiation at 53.7 nm is neglected. Because of the short radiative lifetimes, we neglect transport of the excited atoms and consider only the steady-state rate equation. With these approximations, the spatially dependent $3\,^1P$ density $n_1(z)$ is given by the solution of

$$\alpha_e^1(E/N)\Gamma_e(z) + \overline{Q}_f^1(E/N)N\Gamma_f(z) + \overline{Q}_+^1(E/N)N\Gamma_+(z) - A(501.6)n_1(z) - k_1Nn_1(z) = 0. \tag{15}$$

Here $\alpha_e^1(E/N)$ is the excitation coefficient for electron production of the $3\,^1P$ state and is calculated from Eq. (4) using $Q_e^1(\epsilon)$, the cross section for electron excitation of He to the $3\,^1P$ state, including radiative and collisional cascade effects [57]. The average cross sections for excitation of the $3\,^1P$ state by ions and fast atoms are $\overline{Q}_+^1(E/N)$ and $\overline{Q}_f^1(E/N)$ as discussed in Secs. III G and III H. The radiative transition

probability for the 501.6 nm transition $A(501.6)$ and other transitions are from Ref. [61]. The net rate for collisional quenching, e.g., excitation transfer to the $3\,^1D$ state and of associative ionization to form He_{2^+}, is $k_1\,N\,n_1$ [56]. For the one-dimensional Maxwellian model of Sec. III B used at high E/N, the coefficient $\alpha_e^1(E/N)$ in Eq. (15) should be replaced by $\overline{Q_e^1}(E/N)N$ and evaluated using Eq. (12). In Sec. III G, we will use Eq. (15) to evaluate effective values of $\alpha_e^1(E/N)$.

The 501.6 nm count rate is $S\{j,(E/N),N,z\} = C_1 A(501.6) n_1(z)$, where the photon detection efficiency C_1 is assumed independent of z. If the photon signal is extrapolated to the position of the anode, where $\Gamma_f(d) = \Gamma_+(d) = 0$, then Eq. (15) gives

$$\alpha_e^1(E/N) = S\{j,(E/N),N,d\}(1 + N/N_0)/(C_1 j/e), \quad (16)$$

where we have replaced $\Gamma_e(d)$ by the total charge flux j/e. The spatially dependent apparent excitation coefficient is then defined by

$$\beta_e^1(E/N,z) = S\{j,(E/N),N,z\}(1 + N/N_0)/(C_1 j/e). \quad (17)$$

The ratio of these coefficients yields Eq. (1) follows when $\alpha_e^1(E/N)_r$ is evaluated at some reference $(E/N)_r$ and gas density N_r.

For the He($3\,^3D$) state, the only radiative decay is to the $2\,^3P$ state by emission of the 587.6 nm line. Collisional coupling to nearby $3\,^1D$ and radiative or collisional cascading from higher states are included in a very much simplified form. The $3\,^3D$ density $n_3(z)$ is given by

$$\alpha_e^3(E/N)\Gamma_e(z) + \overline{Q_f^3}(E/N)N\Gamma_f(z) + \overline{Q_+^3}(E/N)N\Gamma_+(z) - A(587.6)n_3(z) - k_3 N n_3(z) = 0. \quad (18)$$

Here $\alpha_e^3(E/N)$ is the spatial excitation coefficient for the $3\,^3D$ state resulting from electron collisions and includes both direct excitation and production by excitation transfer. Its determination is discussed in Sec. III F. The average cross sections for excitation of the $3\,^3D$ state by fast atoms and by ions are $\overline{Q_f^3}(E/N)$ and $\overline{Q_+^3}(E/N)$ and are discussed in Secs. III G and III H. The radiative transition probability for the 587.6 nm line $A(587.6)$ is from Ref. [61]. The rate coefficient for collisional excitation transfer to nearby levels and for associative ionization is k_3 [62]. The effects of production by collisions and radiative cascading from the $n\,^3L$ states with $n \geq 4$ are included in $\alpha_e^3(E/N)$, as discussed below. The coefficients $\alpha_e^3(E/N)$ and $\beta_e^3(E/N,z)$ for the 587.6 nm line are defined by analogy with those for the 501.6 nm line and are consistent with Eq. (1).

In order to solve the equations of this section for the spatially-dependent, steady state photon fluxes, we need the set of cross sections and reaction coefficients appearing in Eqs. (2)–(18). These are reviewed in Secs. III F through III H.

F. Electron-He cross sections and excitation coefficients

The theoretical electron-He excitation coefficients used in the present paper at low E/N are calculated using electron energy distributions from solutions to the electron Boltzmann equation calculated using a simplified cross section set found to reproduce measured electron transport and ionization coefficients [19]. They are available on the Web [63] and will not be repeated here. The electron energy distributions from such calculations are folded into more recently compiled excitation cross sections for the $3\,^1P$ and $3\,^3D$ excited states [64]. The resultant ionization coefficients α_e^i, excitation coefficient for the $3\,^1P$ state α_e^1, and direct excitation coefficient for the $3\,^3D$ state α_e^3 are shown by the crosses in Fig. 4.

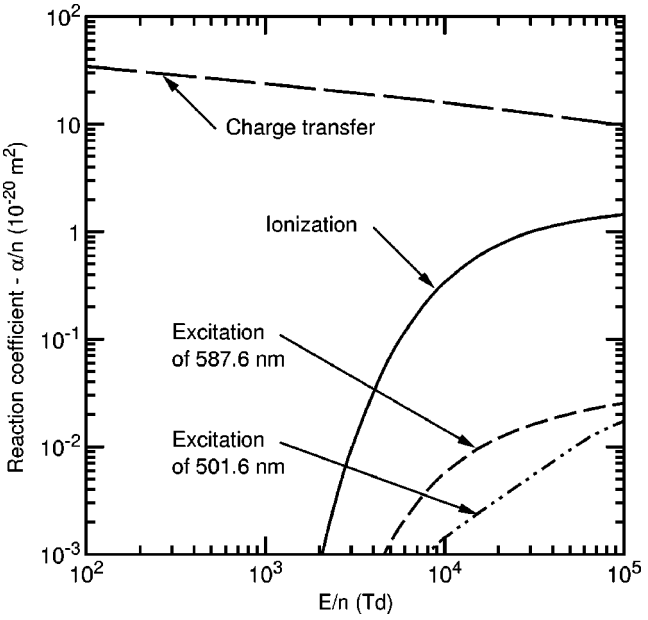

FIG. 6. Reaction coefficients for He^+ in He.

It is critical that we take into account the transfer of excitation from the singlet states of He to the triplet states, such as the $3\,^3D$ state. In order to do this, we must extrapolate the results of the beam excitation experiments of Jobe and St. John [57] and the excited state fluorescence experiments [56,65] to about a decade higher pressure. We assume that most of the transfer can be accounted for by collisional excitation transfer from the $n\,^1P$ state to the $n\,^1F$ and $n\,^3F$ states where $n \geq 4$ and then by collision and radiation to the $3\,^3D$ state. Figure 5 shows that because of excitation transfer, the excitation cross section for the 587.6 nm line appears to approach one third of that for the 501.6 nm line at high pressures. In the pressure range of our experiments indicated by the vertical dotted lines, this fraction remains constant. We therefore approximate the excitation transfer effects at our pressures near 1 Torr by adding a fraction (1/3) of the electron excitation coefficient for the $3\,^1P$ state to that for the $3\,^3D$ state. The resultant excitation coefficient for the $3\,^3D$ state is shown by the dashed curve in Fig. 4.

G. He^+ cross sections and electron yield at cathode

The charge transfer, ionization, and excitation coefficients versus E/N that we have assembled from the literature for He^+ collisions with He are shown in Fig. 6. These coeffi-

cients have been obtained by averaging the respective cross sections over the one-dimensional Maxwellian energy distribution calculated to occur when He^+ drifts through He at the stated E/N, i.e., Eq. (12). Experimental symmetric charge transfer cross sections for He^+-He collisions prior to 1991 have been reviewed by Sakabe and Izawa [66,67]. At energies below 8 eV and E/N below 2 kTd, we have adopted the empirical fit [55] shown in Fig. 6 based on mobility data by Helm [34]. At higher energies we have used an average of the somewhat scattered experimental results, rather than theory [66,67]. The ionization cross section for He^+ on He is from Gilbody *et al.* [68]. The cross sections for excitation of 501.6, 587.6, and 53.7 nm lines in He^+-He collisions are from Okasaka *et al.* [69]. The 501.6 nm data are corrected for the branching ratio to obtain the $3\,^1P$ excitation cross section. Borst *et al.* [70] obtained a cross section for excitation of the $2\,^3S$ metastable state at energies up to 2 keV, while Utterbach [71] obtained evidence of significant metastable excitation near threshold. Evans and Lane [72] reviewed and extended theory for metastable excitation. The experimental values for the ionization coefficient for He^+-He collisions obtained by Townsend and Yarnold [36] at E/N from 80 to 200 Td are one to two orders of magnitude too small to plot in Fig. 6 but are many orders of magnitude larger than any reasonable extrapolation of our calculated values to such low E/N.

The empirical fit to the experimental data of Hayden and Utterbach [73] used for the electron yield per He^+ ion γ_i is

$$\gamma_i = 0.24 + 1.2(\epsilon/1000)^{1.7}/[1 + (\epsilon/1800)^2]^{0.8}, \qquad (19)$$

where ϵ is the ion energy in eV. The γ_i is converted to a function of E/N using Eq. (13). We have multiplied Eq. (19) by an empirical electron escape probability to get the net electron production per ion. There is a large scatter in published data [9,74], and we have approximated it by the same function as for electrons in Ar [29].

H. Fast He atom-He cross sections and reaction coefficients

The energy loss, ionization, and excitation coefficients versus E/N for fast He collisions with He are shown in Fig. 7. These coefficients have been obtained by averaging the respective cross sections over the one-dimensional Maxwellian energy distribution calculated to occur when He^+ drifts through He at the stated E/N and undergoes symmetric charge transfer collisions to produce the fast He. The cross sections for elastic and inelastic He-He collisions have been reviewed and extended [55]. The viscosity cross section determines the rate of elastic energy loss, and in our model, a viscosity collision results in the loss of a fast He atom. At energies below about 40 eV this cross section was calculated from a modification of published intermolecular potential data [75]. At higher energies corrections were made for inelastic collisions based on experimental differential scattering data [76]. We use the sum of the elastic and inelastic viscosity cross sections shown by long dashes. The excitation of the 501.6 and 587.6 nm lines has been measured by Kempter *et al.* [77,78]. Excitation of the $2\,^1P$ state and ionization have been calculated by Gauyacq [60], where because of symmetry considerations we have noted [55] that the theoretical cross sections have to be multiplied by a factor of 2 for comparison with experiment. The ionization cross section has been measured by Hayden and Utterback [73].

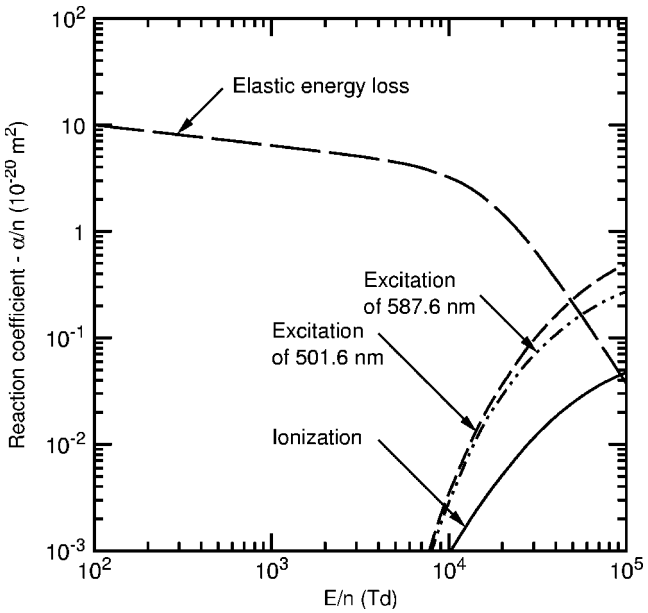

FIG. 7. Reaction coefficients for fast He in He.

The empirical fit to the experimental data of Hayden and Utterback [73] used for the electron yield per fast He striking the cathode γ_f is

$$\gamma_f = 0.06\exp[-11000/(E/N)] + 0.08\exp[-30000/(E/N)] + 1.3\exp[-50000/(E/N)], \qquad (20)$$

where E/N is in Td. The conversion from fast atom energy to E/N used Eq. (13). Again, we have approximated the electron escape probability by the same function as for electrons in Ar [29].

IV. COMPARISON OF MODEL AND EXPERIMENT

In this section we present the results of fitting our experimental emission data to our model at low E/N, where excitation coefficients calculated using local field theory apply, and then examine the consequences of comparing the model and experiment at higher E/N.

The calibration procedure for the detection system represented by Eq. (1) yields the points of Fig. 8 and 10 as described in the following subsections. The "apparent excitation coefficients" β/N shown in these figures are the number of excitation events per unit time and per gas atom normalized to the total charged particle flux density [1]. Alternatively, these coefficients can be regarded as the number of excitation events per unit distance in the field direction per charged particle of either sign passing the observation point and normalized to the gas density. At high E/N, because of changes in the velocity distribution of the electrons with position and because of the spatial variations in the production

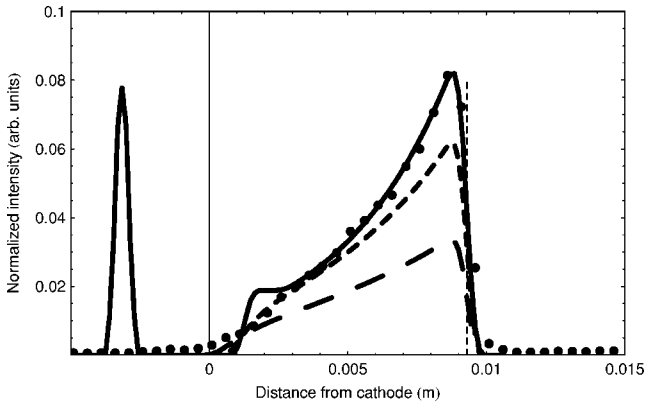

FIG. 8. Apparent emission probability at 501.6 nm from helium at 446 Td and 1.7 Torr. The ● points show our experimental results. The solid, long dashed, and short dashed curves show the results of our local field, single-beam, and Maxwellian beam models, respectively. The Gaussian-like curve at the left shows the spatial sensitivity used to simulate the effect of a finite slit width.

of excited atoms by electrons, ions, and fast atoms, it is not possible to express the experimental results in terms of a spatially independent excitation coefficient per unit electron flux as is conventionally done [1] at the lower E/N. We therefore use the intensity calibrations given by Eq. (1) for the 501.6 nm and 587.6 nm lines to normalize the remainder of the data in Figs. 2 and 3. Examples of the scaled apparent excitation coefficients are shown by the points in Figs. 8–11.

A. Ionization coefficients

Ionization coefficients derived from straight-line-fits to logarithmic plots of experimental emission versus distance data are shown by the solid circles and diamonds in Fig. 4. These coefficients are to be compared to the values obtained by solving the electron Boltzmann equation [79] as shown by the $\times$ symbols and with an average of previous experimental and theoretical data [7,8,17,22–25] as shown by the portion of the upper solid curve for $E/N<800$ Td. We also show by $+$ symbols the ionization coefficients calculated by Hayashi using Monte Carlo techniques [9]. Because Hayashi's calculated ionization coefficients for $E/N>600$ Td vary with distance, we have shown his apparent α_i/N at values of $p_0 d$ (1 Torr cm) typical of our experiments. We have not attempted to extract effective ionization coefficients from the calculations of current growth of Pace and Parker, because of the difficulty of separating gas ionization and cathode emission effects [28].

B. Excitation of 501.6 nm emission

The solid squares of Fig. 4 show apparent excitation coefficients β/N derived by extrapolating 501.6 nm emission data to the anode and applying Eq. (1) to normalize the data to the low E/N data. These excitation coefficients are to be compared to the results of our Boltzmann calculation as shown by the associated crosses. Superficially, one is not surprised that because of the similarity of the energy dependencies of cross sections for production of 501.6 nm photons

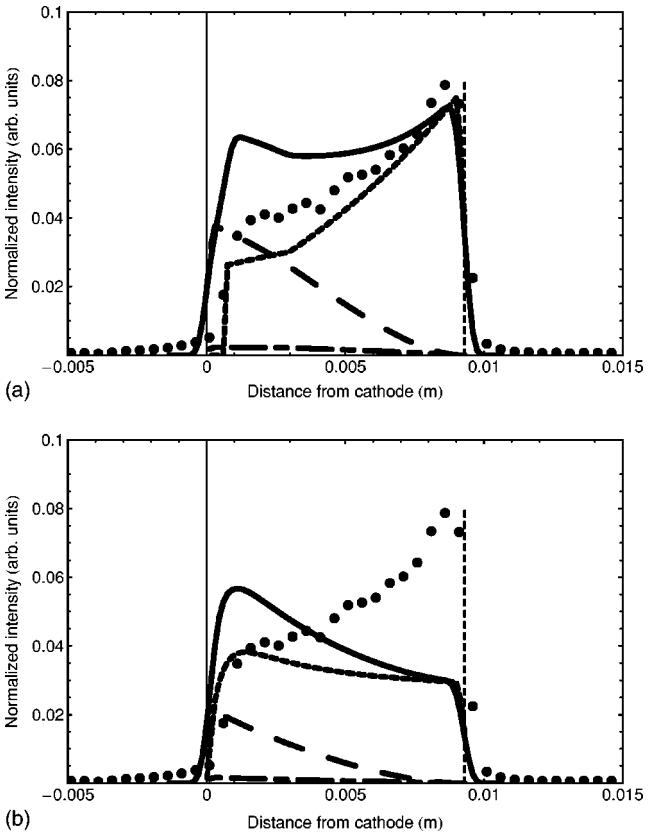

FIG. 9. Apparent emission probability at 501.6 nm from helium at 7.2 kTd and 1.05 Torr. The ● points show our experimental results. The curves in (a) and (b) show the results of our local field and nonequilibrium models, respectively. The solid curves are the calculated and smoothed total emission. The short-dashed, dot-dashed, and long-dashed curves present the contributions of excitation by electrons, ions, and fast atoms, respectively.

and of electron-ion pairs in ionizing collisions by electrons [21] that this experimental excitation coefficient has a dependence on E/N similar to that for ionization. Potential problems with this simple expectation are evident in the departure

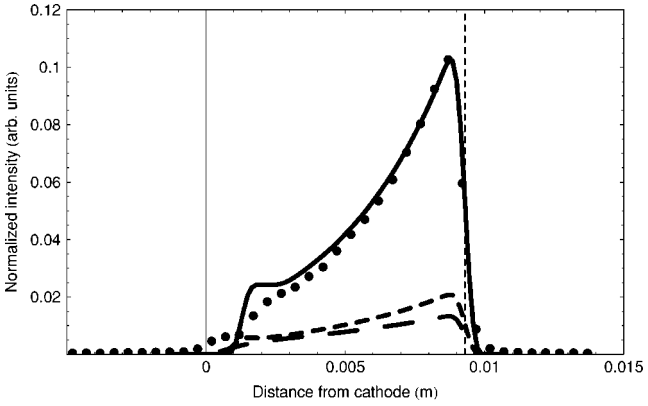

FIG. 10. Apparent emission probability at 587.6 nm from helium at 740 Td and 1.49 Torr. The ● points show our experimental results. The solid, long dashed, and short dashed curves show the results of our local field, single-beam, and Maxwellian beam models, respectively.

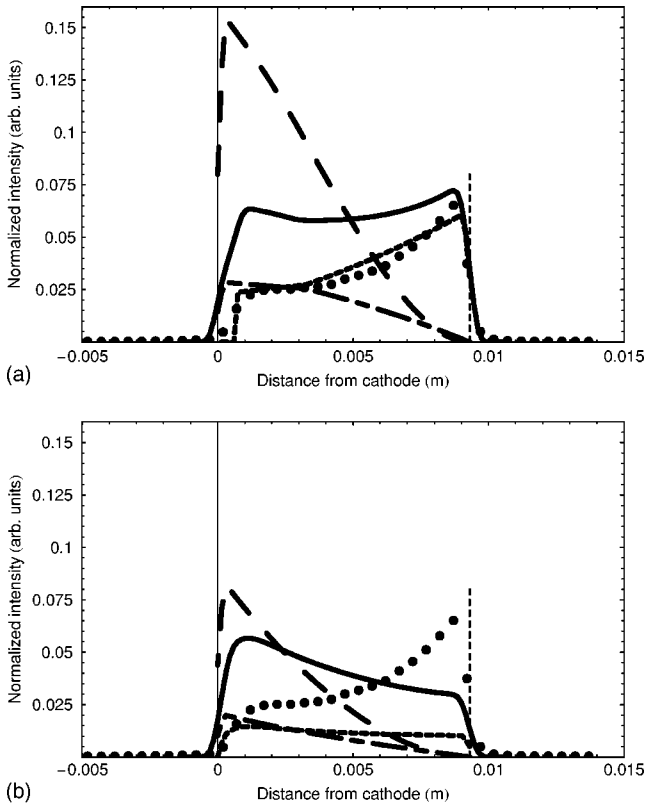

FIG. 11. Apparent emission probability at 587.6 nm from helium at 8.8 kTd and 0.96 Torr. The ● points show our experimental results. The curves in (a) and (b) show the results of our local field and nonequilibrium models, respectively. The curves are designated as in Fig. 9.

of the experimental β/N values from the Boltzmann and Monte Carlo calculations at the higher E/N.

Figure 8 shows the spatially dependent, apparent emission probability at 501.6 nm from helium at 446 Td. The points show our experimental results, while the solid and dashed curves show results of our local field and nonequilibrium model for electrons. The theory is scaled to our pressure using Eq. (1) and a quenching density of 2.1×10^{22} m^{-3} [80]. The calculated heavy particle excitation is too small to be seen. As discussed in Sec. II, we have calibrated the detection system at 501.6 nm by adjusting the magnitude of the experimental data to fit the theory (solid curve). In Fig. 8 the calculated emission has been averaged over the estimated instrument profile shown at the left and over a function of similar width that accounts for obscuration of the edges of the gap by the electrodes. The agreement of the emission calculated using the local field model with the experimental spatial dependence is expected because of the applicability of the steady state Boltzmann model. The predictions of our single-beam model (short dashes) are much better than expected, while one-dimensional, Maxwellian model for electrons (long dashes) are roughly a factor of two too small in magnitude and shows much too small an electron flux growth by ionization. The dashed curves show that the expected nonequilibrium effects near the cathode occur naturally for the single-beam and 1D Maxwellian nonequilibrium models. Comparison of the solid curve with experiment indicates that our step-function approximations to the spatially dependence of the ionization and excitation coefficients used with the local field model are reasonable.

The points of Fig. 9 show the spatially dependent, apparent emission probability at 501.6 nm from helium at 7.2 kTd. The solid curve of Fig. 9(a) shows that the predictions of the local field model are surprisingly good, while the solid curve of Fig. 9(b) shows that the nonequilibrium model considerably underestimates the growth of emission toward the anode. The decrease in the electron excitation cross section for electron "temperatures" above about 100 eV, which occurs about 0.5 mm from the cathode, just balances the increase in electron flux (not shown). The contributions of electrons (short dashes) and fast atoms (long dashes) are overestimated near the cathode. The contribution by ions (dot-dash) is small.

The predictions of the single-beam model for electrons (not shown) are poor at 7.2 kTd in He. According to this model, the electron excitation peaks very close to the cathode as the electrons pass through the energy of maximum excitation cross section while undergoing nearly free-fall motion in the applied electric field. The failure of the single-beam model for electrons at the highest E/N in He, while succeeding for electrons at similar E/N in Ar [3], can be understood when one notes that the cross sections for excitation and ionization in He are almost an order of magnitude smaller than those for Ar. Thus, the effective E/N for He are almost an order of magnitude larger than for Ar. We have no explanation for the relative success of the local field model for He shown in Fig. 9(a). Unfortunately, we did not test the local field model at very high E/N for electrons in Ar.

C. Excitation of 587.6 nm emission

Relative apparent excitation coefficients $\beta_e^3(E/N,z)$ are calculated from data such as that of Fig. 3 using Eq. (1). The exponentially increasing component of these spatial distributions, i.e., the component of emission caused by electrons, are then extrapolated to the position of the anode to obtain the relative values of $\alpha_e^3(E/N)$ shown by the triangles in Fig. 4. The E/N dependence of these values is roughly the same as the experimental points for the 501.6 nm emission, rather than the E/N dependence of the calculated direct electron excitation shown by the lowest solid curve and crosses. According to the model of Sec. III E, the excess emission at the higher E/N is the result of excitation transfer from the $n\,^1P$ states with $n\geqslant 4$. We have not preformed the level-by-level calculations appropriate to this model. Instead, from Sec. III F, we assume that the effective theoretical 587.6 nm excitation coefficient $\alpha_e^3(E/N)$ is one-third $\alpha_e^1(E/N)$ plus the calculated direct 587.6 nm excitation. This empirical approximation to the theoretical 587.6 nm excitation coefficient for the local field model is applied to all E/N to obtain the dashed curve of Fig. 4. The experimental apparent excitation coefficient data for the 587.6 nm line for 460 and 740 Td, (triangles) are then scaled to the $\alpha_e^3(E/N)$ theory. This scaling step places all of the 587.6 nm data (triangles) on an absolute scale. The sum of one third of the 501.6 nm excitation cross section plus any direct excitation is also used

for 587.6 nm excitation in the nonequilibrium models of electron excitation and of heavy particle excitation.

Figure 10 shows the spatially dependent, apparent emission probability at 587.6 nm from helium at 740 Td. The points show our experimental results after normalization using a sensitivity derived as described in the previous paragraph. The smooth curve shows our local field model results. A quenching density of 8.9×10^{23} m^{-3} was used [81]. Because we have normalized experiment and theory at the anode, this comparison really only tests the spatial dependence of the emission and depends primarily on the growth of electron flux, i.e., on the ionization coefficient. For the 587.6 nm line the predictions of both the single-beam and Maxwellian beam models, including excitation transfer, are too small by a factor of about 4.

Figure 11 shows the spatially dependent, apparent emission probability at 587.6 nm from helium at 8.8 kTd. The points show our experimental results normalized using the scaling factor from Fig. 10. The smooth curves in Fig. 11(a) are calculated using our local field model, while the smooth curves in (b) show our 1D Maxwellian beam model results. The upper graph shows that the calculated electron excitation is about right, while the heavy ion and fast atom excitation are too large by roughly a factor of 6. From the lower graph the electron excitation is roughly a factor of 4 too small, and is nearly constant with position as the result of a balance between a decreasing excitation cross section and an increasing electron flux. The lower ion and fast atom production of 587.6 nm excitation predicted by the 1D Maxwellian model is too large by about a factor of 4. If we had used the large fast atom attenuation cross section from Ref. [13], the predicted 587.6 nm excitation near the cathode for both of these models would be much smaller. The theoretical results for the single beam model (not shown) again peak close to the cathode as expected for nearly free fall motion of the electrons.

V. BREAKDOWN AND DISCHARGE MAINTENANCE AT LOW CURRENTS

Experimental values of the decrease in discharge voltage versus current for low current, steady state discharges in He at pressures of 1.5 and 2 Torr are shown in Fig. 12. Here we measure the decrease in discharge voltage from the breakdown value at close to zero current so as to minimize problems with the slowly drifting discharge voltages caused by changing cathode properties. In addition, we show a few points obtained from overdamped transient voltage and current waveforms [47,82]. The data of Fig. 12 cover a p_0d range of 1.5 to 3 Torr cm, corresponding to an E/N range of 150 to 500 Td and, according to our model, $\gamma_i=0.24$ and γ_f is negligible. Over the full range of breakdown voltages in Fig. 13, we measure negative voltage changes within the estimated uncertainty of the data but the high voltage data are too limited to allow assigning meaningful slopes.

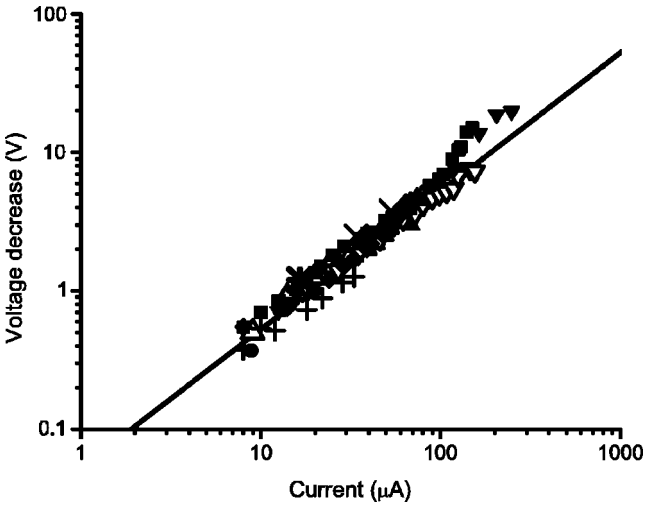

FIG. 12. Experimental decrease in discharge voltage versus current for low current discharges in He. For the steady state data the symbols, pressures in Torr, and voltages in V at zero current are (△, ▽), 1.6±0.1, 220±10 and (◆, ●, ▲, ▼, ■), 2±0.2, 177±5, where different symbols are for different runs. The data from transient waveforms are ∗, 1.5, 210, ×, 2, 171, and +, 3, 156. The straight line represents a constant voltage decrease to current ratio of 53 V/mA.

Theory [83–87] predicts a linear decrease in voltage with increasing current at low currents because of the increase in space-charge electric field near the cathode and the resultant increase in the ion energy and in γ_i. The discharge currents in our experiments are small enough so that multistep ionization phenomena are not significant. Similar linear de-

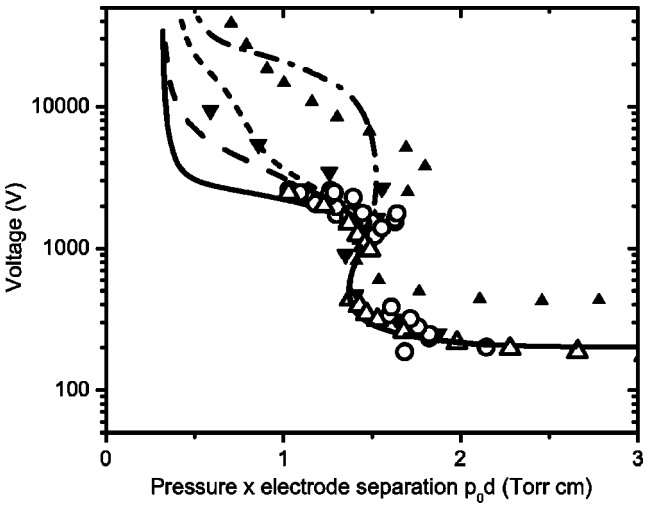

FIG. 13. Experimental values of the discharge voltage versus the product of pressure and electrode separation p_0d at breakdown or for low current, steady state discharges in He. The solid, short dashed, and chain curves give our predictions with heavy-particle-induced electron emission and collisional ionization by ions and fast atoms, no fast atom effects, and only ion-induced electron emission. The long dashed curve is the same as the solid curve except that we used the fast-atom cross sections of Ref. [13]. The symbols, cathode surface, and references are ○, stainless steel, this paper, ▲, steel, [90], ▼, steel, [28] and △, copper, [13].

creases in voltage with increasing current have been found for Ne [83], Ar [85,88], and other gases. Because of the near constancy of our assumed electron yield per ion, the calculated dV/di is very sensitive to the assumed electron loss by backscattering to the cathode [29,74], and can be much larger or much smaller than shown in Fig. 12. We cannot account for the positive dV/di found by Hartmann *et al.* [13] for He at average current densities and p_0d values overlapping the lower values of Fig. 12. A possibility is differences in γ_i and/or reflection of backscattered electrons at their copper versus our stainless steel cathodes. Penning [89] found positive dV/di for the lower voltage branch and negative dV/di for the higher voltage branch. See Fig. 13.

Our experimental values of the discharge voltages for steady state discharges in He, extrapolated to very low currents, are plotted versus the p_0d as circles in Fig. 13. We show the results of earlier experiments in He [13,28,90], where the data of Ref. [13] were obtained by extrapolation of steady state voltages to zero current. We have omitted the very early data of Penning [89] and some other data are sampled for clarity. The lower and very high breakdown voltages are obtained by raising the voltage slowly at fixed pressure. Intermediate voltage data are usually obtained by raising the pressure at fixed voltage. Within our large scatter, our experimental results are in good agreement with those of Hartmann *et al.* [13]. The differences between our results and those of Guseva [90] may result from the cleaner cathodes typically used by her group [91].

The solid curve of Fig. 13 show the breakdown voltages versus p_0d calculated for He using Eqs. (2)–(5). Thus, the model includes electron, ion, and fast atom impact ionization and ion and fast atom induced electron emission from the cathode. The differential equations were integrated from the anode to the location of the cathode as determined by the condition that the electron energy decreases from an assumed anode value to a few eV at the cathode. In order to obtain a better fit to the experimental breakdown data, we have made small changes ($\sim$20%) in the effective ionization coefficient given in Fig. 4 at E/N near 1.5 kTd. Typical effective values of γ_i required by our breakdown model vary from 0.25 at 500 Td to $\approx$0.7 at 8 kTd. We find that the fast atom induced electron emission from the cathode is important in obtaining a reasonable fit to experiment for breakdown voltages above 1 kV. Hartmann *et al.* [13,92,94,95] found only a small contribution from fast atoms, and calculated voltages significantly higher than their experiment at low p_0d. The short dashed curve shows predictions of our model with no fast atom effects, while the chain curve shows breakdown with no fast atom effects and no ion-induced ionization, i.e., including only electron impact ionization and ion-induced electron emission at the cathode. The long dashed curve shows the effect of increasing the fast atom scattering cross section to the values of Ref. [13]. We have also calculated breakdown voltages for the original Townsend model [51,52] from Sec. III A, i.e., the only ionization is by electrons and He^+ ions and no electrons are released from the cathode. The resultant breakdown voltages (not shown) are then $\approx$3000 V for $p_0d > 2$ Torr cm and rise to very large voltages at p_0d below 1 Torr cm. These calculations suggest that if it were not for the large contribution of fast atom-induced electron emission, the breakdown voltages at our p_0d would be high enough so that the effects of ionization of He by He^+ would be observed.

VI. DISCUSSION

The experiments and models presented in this paper cover the transition from (a) moderate E/N, where the electrons are in collisional equilibrium with the electric field and the gas and the ion energies are only a few eV, to (b) very high E/N, where the electrons have few collisions with the gas and the ion and, especially, fast atom energies are large enough to yield significant excitation and ionization. At E/N below 1 kTd the observed magnitude and/or spatial dependence of the 501.6 and 587.6 nm emission are consistent with the excitation and ionization expected of electrons with a steady state energy distribution determined by the local electric field and collisions with the gas. The excitation of 587.6 nm emission by fast atoms becomes comparable with electron excitation at E/N above 4 kTd, while the excitation of the 501.6 nm line is primarily by electrons even at E/N of 7 kTd. At the higher E/N, the local field model of the electrons gives better agreement with experiment than do either of the simplified nonequilibrium models that we tried. A Monte Carlo or equivalent model of the electrons is needed.

A second important result of this experiment is the importance of efficient excitation transfer from the $n\,^1P$ states to other excited states, such as the $3\,^3D$ state that we detect. The excitation transfer is easier to observe in the triplet system because of the absence of excitation by the high energy electrons dominant at our relatively high E/N.

A third key result is the importance of excitation near the cathode and electron emission at the cathode by fast He atoms produced by symmetric charge exchange of He^+ with He at high E/N. Here we found that the use of recently derived scattering cross sections greatly increases the contributions of the fast atoms to the observed to the calculated excitation. The longer atom mean-free-paths point to the desirability of Monte Carlo or equivalent models.

Finally, the analyses of breakdown and low-current discharge maintenance voltage data presented in this paper demonstrate the importance of fast atoms in the production of electrons at the cathode. This conclusion depends critically on the cross sections for fast atom scattering used in the model. We were not able to see evidence of the ionization of He by He^+.

The experiments and analyses presented in this paper lead to the suggestion that one observe the time dependence of spectrally and spatially resolved emission in uniform and nonuniform electric fields. Such observations [4] provided direct evidence for the importance of excitation in collisions of fast Ar atoms with the background Ar. We also propose the measurement of ionization coefficients as a function of pressure at moderately high E/N so as to see the effects of molecular ion formation by associative ionization from excited states of He.

ACKNOWLEDGMENTS

The authors would like to acknowledge many helpful discussions with A. C. Gallagher and Z. Lj. Petrović. A.V.P. wishes to thank B. A. Fast and M. E. Tamisiea for advice on the use of Mathematica©. This work was supported in part by the National Institute of Standards and Technology. B.M.J. acknowledges support by the MNT Serbia, Project No. 1443.

[1] B. M. Jelenkovic and A. V. Phelps, Phys. Rev. A **36**, 5310 (1987).
[2] A. V. Phelps, B. M. Jelenković, and L. C. Pitchford, Phys. Rev. A **36**, 5327 (1987).
[3] A. V. Phelps and B. M. Jelenkovic, Phys. Rev. A **38**, 2975 (1988).
[4] D. A. Scott and A. V. Phelps, Phys. Rev. A **43**, 3043 (1991).
[5] Z. Lj. Petrović, B. M. Jelenković, and A. V. Phelps, Phys. Rev. Lett. **68**, 325 (1992).
[6] Z. Lj. Petrović (private communication).
[7] M. J. Druyvesteyn and F. M. Penning, Rev. Mod. Phys. **12**, 87 (1940).
[8] T. Itoh and T. Musha, J. Appl. Phys. **31**, 744 (1960); J. Phys. Soc. Jpn. **15**, 1675 (1960).
[9] M. Hayashi, *Proc. Fourth IEE Int'l. Conference on Gas Discharges*, *University College of Swansea*, (IEEE, London, 1976), p. 195; M. Hayashi, J. Phys. D **15**, 1411 (1982).
[10] P. Segur, M. Yousfi, J. P. Boeuf, E. Marode, A. J. Davies, and J. G. Evans, in *Electric Breakdown and Discharges in Gases*, edited by E. E. Kunhardt and L. H. Leusen (Plenum, New York, 1981), p. 331.
[11] J. Fletcher, J. Phys. D **18**, 221 (1985).
[12] E. A. Volkova, V. V. Ivanov, E. Yu. Melkumova, A. M. Popov, O. B. Popovicheva, and T. V. Rakhimova, Fiz. Plazmy **18**, 911 (1992) [Sov. J. Plasma Phys. **18**, 474 (1992)].
[13] P. Hartmann, Z. Donkó, G. Bàno, L. Szalai, and K. Rózsa, Plasma Sources Sci. Technol. **9**, 183 (2000). Our only point of disagreement is that their choice of elastic scattering cross sections for He-He collisions as equal to the "total" cross section is much too large at high energies and should have been assumed equal to the viscosity cross section. See Ref. [63]. Our smaller elastic scattering cross section allows the fast atoms to produce more electrons at the cathode and results in a better fit of theoretical and experimental breakdown data.
[14] J. H. Ingold, Phys. Rev. A **43**, 3086 (1991).
[15] R. Winkler, G. Petrov, F. Sigeneger, and D. Urlandt, Plasma Sources Sci. Technol. **6**, 118 (1997).
[16] K.-U. Riemann, Phys. Rev. A **46**, 4717 (1992).
[17] L. M. Chanin and G. D. Rork, Phys. Rev. **133**, A1005 (1964).
[18] J. Fletcher and P. H. Purdie, Aust. J. Phys. **40**, 383 (1987).
[19] A. V. Phelps, Phys. Rev. **117**, 619 (1960).
[20] I. M. Bortnik, Zh. Tekh. Fiz. **38**, 1016 (1968); **38**, 1026 (1968); [Sov. Phys. Tech. Phys. **13**, 769 (1968); **13**, 777 (1968)].
[21] L. L. Alves and C. M. Ferreira, J. Phys. D **24**, 581 (1991).
[22] J. Dutton, J. Phys. Chem. Ref. Data **4**, 577 (1975).
[23] D. K. Davies, F. Llewellyn Jones, and C. G. Morgan, Proc. Phys. Soc. London **80**, 898 (1962).
[24] M. H. Hughes, J. Phys. B **3**, 1544 (1970).
[25] A. E. D. Heylen and T. J. Lewis, Proc. R. Soc. London, Ser. A **271**, 531 (1963).
[26] G. Auday, Ph. Guillot, J. Galy, and H. Brunet, J. Appl. Phys. **83**, 5917 (1998); G. Auday, Ph. Guillot, and J. Galy, *ibid.* **88**, 4871 (2000).
[27] D. K. Davies, F. Llewellyn Jones, and C. G. Morgan, Proc. Phys. Soc. London **83**, 137 (1964).
[28] A. B. Parker and P. C. Johnson, Proc. R. Soc. London, Ser. A **325**, 511 (1971); J. D. Pace and A. B. Parker, *Third Int'l. Conf. on Gas Discharges* (IEEE, London, 1974), p. 91.
[29] A. V. Phelps and Z. Lj. Pterović, Plasma Sources Sci. Technol. **8**, R21 (1999).
[30] J. E. Lawler, Phys. Rev. A **32**, 2977 (1985).
[31] H. B. Milloy and R. E. Robson, J. Phys. B **6**, 1139 (1973).
[32] D. Piscitelli, A. V. Phelps, J. de Urquijo, E. Basurto, and L. C. Pitchford, Phys. Rev. E **68**, 046408 (2003).
[33] S. L. Lin, L. A. Viehland, E. A. Mason, J. H. Whealton, and J. N. Bardsley, J. Phys. B **10**, 3567 (1977).
[34] H. Helm, J. Phys. B **10**, 3683 (1977).
[35] M. V. V. S. Rao, R. J. Van Brunt, and J. K. Olthoff, Phys. Rev. E **54**, 5641 (1996).
[36] J. S. Townsend and G. D. Yarnold, Philos. Mag. **18**, 594 (1934).
[37] H. Neu, Z. Phys. **154**, 423 (1959); **155**, 77 (1959).
[38] W. D. Davis and T. A. Vanderslice, Phys. Rev. **131**, 219 (1963); A. V. Bondarenko, Zh. Tekh. Fiz. **43**, 821 (1973) [Sov. Phys. Tech. Phys. **18**, 515 (1973)].
[39] K. N. Ul'yanov, Teplofiz. Vys. Temp. **16**, 1121 (1978) [High Temp. **16**, 955 (1978)]; K. N. Ul'yanov and A. B. Tskhai, *ibid.* **19**, 41 (1981) [*ibid.* **19**, 32 (1981)].
[40] D. G. Armour, H. Valisadeh, F. A. H. Soliman, and G. Carter, Vacuum **34**, 295 (1984).
[41] R. T. C. Tsui, Phys. Rev. **168**, 107 (1968); I. Abril, A. Gras-Marti, and J. A. Valles-Abarca, Phys. Rev. A **28**, 3677 (1983); I. Abril, A. Gras-Marti, and J. A. Valles-Abarca, J. Phys. D **17**, 1841 (1984); J. Rickards, Vacuum **34**, 559 (1984).
[42] W. H. Long, Jr., Air Force Aero Propulsion Laboratory, Report No. AFAPL-TR-79-2038, 1979 (unpublished); H. Chatham and A. Gallagher, J. Appl. Phys. **58**, 159 (1985).
[43] P. Hartmann, H. Matsuo, Y. Ohtsuka, M. Fukao, M. Kando, and Z. Donkó, Jpn. J. Appl. Phys., Part 1 **42**, 3633 (2003).
[44] B. M. Jelenković and A. V. Phelps, Bull. Am. Phys. Soc. **43**, 1432 (1998).
[45] Vacuum grade POCO graphite, Poco Graphite, Inc., 300 Old Greenwood Rd., Decatur, Texas 76234.
[46] D. L. Albritton, At. Data Nucl. Data Tables **22**, 1 (1978).
[47] B. M. Jelenković, K. Rózsa, and A. V. Phelps, Phys. Rev. E **47**, 2816 (1993).
[48] F. J. De Hoog and J. Kasdorp, Physica (Amsterdam) **34**, 63 (1967); A. K. Bhattacharya, Phys. Rev. A **13**, 1219 (1976); J. Appl. Phys. **50**, 6207 (1979).
[49] Because of the difficulty in extracting the electron excitation component of the 587.6 nm emission from the sum of the elec-

tron and heavy-particle components for the highest E/N of Fig. 3, we have omitted that data from Fig. 4.
[50] M. I. Datsiev and Yu. I. Belyakov, Zh. Tekh. Fiz. **39**, 1128 (1969) [Sov. Phys. Tech. Phys. **14**, 849 (1969)]; T. D. Madey and J. T. Yates, Jr., J. Vac. Sci. Technol. **8**, 525 (1971).
[51] J. S. Townsend, *Electricity in Gases* (Clarendon, Oxford, 1915), p. 314.
[52] L. B. Loeb, *Fundamental Processes of Electrical Discharge in Gases* (Wiley, New York, 1939), p. 372.
[53] C. B. Opal, W. K. Peterson, and E. C. Beaty, J. Chem. Phys. **55**, 4100 (1971).
[54] G. W. Stuart and E. Gerjuoy, Phys. Rev. **119**, 892 (1960).
[55] A. V. Phelps, Bull. Am. Phys. Soc. **47**, 41 (2002) and (unpublished). See Ref. [63] for some He-He results.
[56] H. F. Wellenstein and W. W. Robertson, J. Chem. Phys. **56**, 1411 (1972).
[57] J. D. Jobe and R. M. St. John, Phys. Rev. A **5**, 295 (1972).
[58] A. V. Phelps, Phys. Rev. **110**, 1362 (1958).
[59] We estimate the escape probability g for the 53.7 nm resonance radiation emitted by the $3\,^1P$ state at our He densities and electrode separation to be $g(53.7)\approx 0.001$, so that the fraction of $3\,^1P$ atoms lost by this process is $g(53.7)A(53.7)/A(501.6)\approx 0.04$. Estimates of the escape factor at higher pressures are difficult because of the transition from natural broadening to collisional or impact broadening in the wings of the line profile. See Ref. [93].
[60] J. P. Gauyacq, J. Phys. B **9**, 3067 (1976).
[61] W. L. Wiese, M. W. Smith, and B. M. Glennon, *Atomic Transition Probabilities* (U.S. Department of Commerce, Washington, D.C., 1966), Vol. 1, p. 11.
[62] J.-C. Gauthier, F. Devos, and J.-F. Delpech, Phys. Rev. A **14**, 2182 (1976).
[63] A. V. Phelps (unpublished). These data are available at ftp://jila.colorado.edu/collision_data. The files /electonneutral/electron.txt, /ionneutral/ionatom.txt and /neutralneutral/atomatom.txt list electron-atom, ion-atom, and atom-atom cross sections.
[64] N. Kato, Y. Itikawa, and K. Sakimoto, "Compilation of Excitation Cross Sections for He Atoms by Electron Impact," National Institute for Fusion Science, Research Report No. NIFS-DATA-15, 1992 (unpublished); T. Kato and R. K. Janev, At. Plasma-Mater. Interact. Data Fusion **3**, 33 (1992).
[65] R. B. Kay and R. H. Hughes, Phys. Rev. **154**, 61 (1967).
[66] S. Sakabe and Y. Izawa, At. Data Nucl. Data Tables **49**, 257 (1991).
[67] S. Sakabe and Y. Izawa, Phys. Rev. A **45**, 2086 (1992).
[68] H. B. Gilbody and J. B. Hasted, Proc. R. Soc. London, Ser. A **240**, 382 (1957).
[69] R. Okasaka, Y. Konishi, Y. Sato, and K. Fukuda, J. Phys. B **20**, 3771 (1987).
[70] P. J. MacVicar-Whelan and W. L. Borst, Phys. Rev. A **1**, 314 (1970).
[71] N. G. Utterbach, Phys. Rev. Lett. **12**, 295 (1964).
[72] S. A. Evans and N. F. Lane, Phys. Rev. A **8**, 1385 (1973).
[73] H. C. Hayden and N. G. Utterback, Phys. Rev. **135**, A1575 (1964).
[74] O. J. Orient, Can. J. Phys. **43**, 422 (1965); A. Békiarian, J. Phys. (France) **29**, 434 (1968); S. Pareathumby and P. Segur, Lett. Nuovo Cimento Soc. Ital. Fis. **26**, 243 (1979); V. P. Nagorny and P. J. Drallos, Plasma Sources Sci. Technol. **6**, 212 (1997).
[75] R. A. Aziz and M. J. Salaman, J. Chem. Phys. **94**, 8047 (1991).
[76] J. C. Brenot, D. Dhuicq, J. P. Gauyacq, J. Pommier, V. Sidis, M. Barat, and E. Pollack, Phys. Rev. A **11**, 1245 (1975).
[77] V. Kempter, F. Veith, and L. Zehnle, J. Phys. B **8**, 1041 (1975). Their pressures were $\approx 5\times 10^{-3}$ Torr but the effective dimension of the collision region appears to have been much smaller than for Fig. 5. These authors found no dependence of the cross section on pressure and made no imprisonment correction.
[78] V. Kempter, G. Riecke, F. Veith, and L. Zehnle, J. Phys. B **9**, 3081 (1976).
[79] L. S. Frost and A. V. Phelps, Phys. Rev. **127**, 1621 (1962).
[80] This estimate is based on the $3\,^1P$ radiative transition probability of 1.338×10^7 s^{-1} appropriate to an optically thick resonance line and the measured collisional loss cross sections of Wellenstein and Robertson [56]. The $3\,^1P$ loss appears to be primarily ($\sim$60%) to the $3\,^1D$ state which, at our pressures, radiates the 667.8 nm line ($\sim$80%), undergoes He_{2^+} formation by associative ionization ($\sim$12%), and the reverse excitation transfer ($\sim$8%). The estimated effect of collisions on the apparent line excitation cross section for 501.6 nm is shown by a dashed curve in Fig. 4. This comparison suggests that the use of the data from Ref. [56] in our simplified model overestimates the effects of quenching.
[81] This is based on the measurements [62] of a two-body rate coefficient of 8×10^{-11} cm^3/s and a radiative transition probability for the $3\,^3D$ state of 7.06×10^7 s^{-1}. The quenching collisions appear to lead to He_2^+ formation by associative ionization as well as excitation transfer. The estimated effect of quenching on the apparent line excitation cross section for 587.6 nm at high pressures is shown by a dashed curve in Fig. 4.
[82] Because of a missing record, these transient data are normalized to the steady state data at one point by assuming a 100:1 voltage divider.
[83] V. N. Melekhin and N. Yu. Naumov, Zh. Tekh. Fiz. **54**, 1521 (1984) [Sov. Phys. Tech. Phys. **29**, 888 (1984)]; V. N. Melekhin, N. Yu. Naumov, and V. Tkackenko, *ibid.* **57**, 454 (1987) [*ibid.* **32**, 274 (1987)].
[84] A. V. Phelps, Z. Lj. Petrović, and B. M. Jelenković, Phys. Rev. E **47**, 2825 (1993).
[85] Z. Lj. Petrović, I. Stefanović, S. Vrhovac, and J. Živković, J. Phys. IV **7**, C4–341 (1997).
[86] S. Živanov, J. Živković, I. Stefanović, S. Vrhovac, and Z. Lj. Petrović, Eur. Phys. J.: Appl. Phys. **11**, 59 (2000).
[87] I. D. Kaganovich, M. A. Fedotov, and L. D. Tsendin, Zh. Tekh. Fiz. **64**, 22 (1994) [Tech. Phys. **39**, 241 (1994)].
[88] I. Stefanović and Z. Lj. Petrovic, Jpn. J. Appl. Phys., Part 1 **36**, 4728 (1997).
[89] F. M. Penning, Phys. Z. **33**, 816 (1932). The helium available to Penning may not have been very pure. Ionization of impurities by metastables has been observed to cause positive voltage-current characteristics at low currents [7].
[90] L. G. Guseva, in *Investigations into Electrical Discharges in Gases*, edited by B. N. Klyarfel'd (Pergamon, New York, 1964), Fig. 3.
[91] B. N. Klyarfel'd, L. G. Guseva, and A. S. Pokrovkaya-Soboleva, Zh. Tekh. Fiz. **36**, 704 (1966) [Sov. Phys. Tech.

Phys. **11**, 520 (1966)].

[92] We suspect the small contribution of fast atoms to the production of electrons at the cathode in the model of Ref. [13] at our higher E/N is because of their use of much too large an elastic scattering cross section. They used the measured total cross section of Ref. [94], which is expected to be much too large. We used the much smaller theoretical viscosity cross section calculated by Phelps [63,95].

[93] A. F. Molisch and B. P. Oehry, *Radiation Trapping in Atomic Vapours* (Clarendon, Oxford, 1998), Chap. 18.

[94] J. E. Jordan and I. Amdur, J. Chem. Phys. **46**, 165 (1967).

[95] A. V. Phelps, Bull. Am. Phys. Soc. **45**, 28 (2000).